Landscape and Ecological Engineering (2019) 15:63–74
https://doi.org/10.1007/s11355-018-0361-2

ORIGINAL PAPER

Monitoring land cover change of a river-floodplain system using high-resolution satellite images

Shiena Okada[1] · Rajendra Khanal[1] · Chihiro Yoshimura[1] · Oliver Saavedra[2] · Masahiro Ryo[1]

Received: 25 November 2017 / Revised: 21 July 2018 / Accepted: 23 July 2018 / Published online: 21 September 2018

Abstract

In this study, a method was developed to monitor habitat structure in river-floodplain systems using high-resolution satellite images from 2010 to 2012 across a 30-km longitudinal section of the Tagliamento River, Northeast Italy. Three ortho-corrected RapidEye satellite images at 5-m spatial resolution and cloud cover of < 1%, with four spectral bands, namely, blue, green, red, and near-infrared, were used for land cover classification by converting pixel values into digital number (DN) distributions. The DN distributions for each band were clustered into separate classes based on correlations among all bands. The rate of unchanged habitat was further calculated as the intersection of all habitats divided by the area of the habitat of interest. The land cover categories were bare alluvium, river water, and vegetation. Bare alluvium was the dominant type, covering 55–75% of land. Vegetation and river water covered a relatively smaller area of the upper part and a larger area of the middle part of the Tagliamento River. The accuracy of this method was greater (> 89%) than that of the conventional unsupervised ISODATA method (> 83%) as river water and vegetation could be differentiated more accurately using this new method. The unchanged area was greater for river water than for vegetation and bare alluvium. These results indicated that habitat distribution changed spatially and temporally, especially for fluvial habitats, while the composition of habitat types was preserved in the middle reaches of the Tagliamento River. This method can be used to continuously and accurately monitor the large-scale spatiotemporal dynamics of habitat structures.

Keywords Habitat turnover · Spatio-temporal dynamics · Land cover classification · Digital number distribution · Pixel value · Tagliamento River

Introduction

River-floodplain systems contain complex habitat structures and are important for river management (Tockner et al. 2008). Habitat structures, described by land cover, habitat type, water qualities, and so forth, influence aquatic faunal communities (García et al. 2011). This is because the heterogeneity of habitat structures such as inflow, parapotamal, plesiopotamal, and palaeopotamal channels affects connectivity, which in turn enriches the diversity of aquatic species in a habitat (Tockner et al. 2010). Habitat structure also contributes to the overall species diversity, or scarcity, of aquatic fauna (Cornell and Lawton 1992; Tilman 1999). For example, the alteration of habitat structure has reduced the abundance of the Japanese eel *Anguilla japonica* Temminck and Schlegel, 1847 in rivers and lakes in Japan (Itakura et al. 2015). The turnover of habitats caused by disturbance, mainly flooding in rivers, is also important for aquatic diversity. Even though aquatic floodplain habitats

Electronic supplementary material The online version of this article (https://doi.org/10.1007/s11355-018-0361-2) contains supplementary material, which is available to authorized users.

✉ Rajendra Khanal
khanal.r.aa@m.titech.ac.jp; rajendra.khanal@gmail.com

Shiena Okada
shienashiena@gmail.com

Chihiro Yoshimura
yoshimura.c.aa@m.titech.ac.jp

Oliver Saavedra
oliversaavedra@upb.edu

Masahiro Ryo
masahiroryo@gmail.com

[1] Department of Civil and Environmental Engineering, School of Environment and Society, Tokyo Institute of Technology, 2-12-1-M1-4, Ookayama, Meguro-ku, Tokyo 152-8552, Japan

[2] Civil and Environmental Research Center, Universidad Privada Bolivia, Cochabamba, Bolivia

are highly dynamic, small changes in the water level and flooding can lead to major habitat changes (van der Nat et al. 2003). Flooding increases similarity in species diversity among aquatic habitats in the river floodplain (Thomaz et al. 2007). However, flooding has resulted in minimal changes in the braiding, sinuosity, and aquatic habitat composition along the Fiume Tagliamento River, Italy (Arscott et al. 2002). Considering the highly dynamic nature of habitat diversity across the river-flood plain, proper management of habitat structure as well as ecological research are crucial for enriching species abundance and diversity (Osugi et al. 2007). Hinojosa-Huerta et al. (2013) showed that a reduction of surface flow led to a reduction in native tree cover but an increase in shrub cover in the riparian corridor delta of the Colorado River, Mexico without significant changes (< 30%) in overall vegetation. In addition, resilience of the dynamic nature of the riparian zone helps to restore its native form.

Researchers still largely rely on field surveys to describe and understand the spatial and temporal dynamics of habitat structures, despite constraints with respect to physical requirements, time, climate conditions, geographical limitations, and costs. Accordingly, there is little information on the dynamics of habitat structures at large spatial and temporal scales (Arscott et al. 2002; van der Nat et al. 2003) and high resolutions. Satellite images and remote-sensing techniques are increasingly used to monitor habitat structures owing to their wide spatiotemporal coverage, effectiveness for data collection, and repeatability (Mertes 2002; Henshaw et al. 2013; Moretto et al. 2013). For instance, high-resolution (0.5–5 m) satellite images have been used to estimate river depth (Legleiter et al. 2004; Kanno et al. 2011) and medium-resolution (10–15 m) satellite images have been used to estimate other water-quality parameters, such as the suspended sediment concentration (Jensen 1996; Xue et al. 2011).

Rosgen (1994) reviewed the classification system for natural rivers based on entrenchment, gradient, width/depth ratio, and sinuosity in various landforms. Satellite images are an important source for land cover classification and have been widely used for the characterization of fluvial habitat, for example, channel morphology and riparian land cover in the River Tay, Scotland (Bryant and Gilvear 1999), distribution and composition of aquatic insect communities effected by forest cover changes in Amazonian forests (Nessimian et al. 2008), aquatic and terrestrial ecosystems in the tundra wetland of the Lena River Delta, Northern Siberia (Schneider et al. 2009), and wetland in the Amazon Basin (Melack and Hess 2010). Changes in flow regime do affect fluvial and riparian habitats, as shown by alternation of habitat features in seasonal streams, and lesser physical alternation in the Sagura Basin, Spain in stable streams where there were no seasonal changes (Belmar et al. 2013). However, the major obstacle to remote-sensing techniques is the resolution, i.e., mainly the presence of shadows, clarity of water, variable substrates and target–sun angle geometry (Marcus and Fonstad 2008). There has been continual recent advancement in remote-sensing techniques as a tool for the classification of riverine habitats (Marcus and Fonstad 2010; Dufour et al. 2013; Whited et al. 2013; Romero et al. 2016).

Most of the proposed methods estimate a single habitat structure in rivers and thus have not been applied to a variety of physical habitats in river-floodplain systems. Henshaw et al. (2013) reported the successful development and application of multispectral Landsat TM satellite data comprising 15- to 30-m spatial resolution satellite images to monitor vegetation dynamics in a river floodplain, but little is known about the dynamics of habitat structures, especially habitat type classifications, at a large spatiotemporal scale and fine spatial resolution. The development of methods to accurately predict ecological responses, changes in biodiversity, and habitat degradation based on high-resolution satellite images would contribute to the design of effective mitigation measures.

Despite numerous studies on the dynamics of habitat structures in river floodplains, habitat type dynamics have not yet been examined at a large spatiotemporal scale. Habitat types have been monitored by field surveys at the reach scale (van der Nat et al. 2003), but more comprehensive monitoring of the spatial heterogeneity of habitat structures is needed. Furthermore, one issue with conventional methods for image classification is the need to select training data to obtain the pixel-value distribution. This selection needs to be done empirically and qualitatively to obtain sufficiently accurate estimates, but is sometimes tricky, as this procedure is based on trial and error. Hence, in the present study, a new method was developed to avoid issues associated with training data selection by converting pixel values into a digital number (DN) distribution. The main objective of this research was to develop a method for monitoring habitat structures in a river-floodplain system based on high-resolution satellite images and to apply this method to the floodplain in the middle reaches of the Tagliamento River, Italy. As a case study, the proposed method quantifies major land cover and aquatic habitat types in a floodplain to understand floodplain dynamics.

Materials and methods

Study area

The target area was the river-floodplain system of the Tagliamento River, located in Northeast Italy. The length of its main stream is approximately 170 km and it drains an area of approximately 2580 km^2 from the Southern Alps to the Adriatic Sea (Tockner et al. 2003). It forms highly complex

and dynamic river-floodplain systems on alluvial fans, and thus is considered the last morphologically intact river in Europe (Müller 1996; Ward et al. 1999; Tockner et al. 2003; Huber and Huggenberger 2015), though anthropogenic alterations have also been described in terms of hydrology and water quality in some sections (Tockner et al. 2008; Bertoldi et al. 2010). The land cover of the target floodplain consists mainly of five types: active riverbed, pasture, grassland, wetland, and cultivated field (Spaliviero 2003); however, the general land cover based on the map of the nineteenth century used in the classification of Spaliviero (2003) needs to be upgraded with the robust and latest information from high-resolution satellite images. Hence, for this study, land cover was categorized into three types and five habitats: river water, vegetated island and bare alluvium; channel, backwaters, ponds, vegetated island and bare alluvium (discussed in detail in "Categorization of habitat types").

The Tagliamento River is characterized by an alpine to Mediterranean climate (Gurnell et al. 2001). November is the wettest and February the driest month (Gurnell et al. 2001). The mean annual precipitation is 1500–1800 mm in the northern catchment area and 1900–2900 mm in the alpine foreland area (Gunawardhana and Kazama 2012). Winter begins with snowfall, which starts in late November or early December, and the snow melts around late March. The river discharge is higher from April to June, and gradually decreases in the summer, probably with the minimum discharge in September. September is also the month with the highest amount of sunshine, with mean monthly sunshine of more than 200 h.

The unconstrained floodplain segments are characterized by a dynamic mosaic of aquatic/terrestrial habitats (Tockner et al. 1999; Arscott et al. 2002), a large number of vegetated islands (Edwards et al. 1999; Gurnell et al. 2001), and a high biodiversity of aquatic communities (Arscott et al. 2005). The floodplains show substantial morphological changes in the network configuration due to flood pulses and unconstrained river banks (Bertoldi et al. 2009). Interestingly, each flooding event along the Tagliamento River spatially reconfigures the habitat composition, but these events do not have substantial effects on the aerial proportion (i.e., composition) of each type of aquatic habitat in each floodplain, leaving a certain combination of major floodplain habitat types available for recolonization (Arscott et al. 2002; van der Nat et al. 2003).

To understand the continuous dynamics of habitat structures at a large spatial scale, the alluvial fan segment about 30 km from Venzone through Cornino and Villuza to Dignano was selected and was divided into five sections, A–E, from north to south (Fig. 1). In addition, three target reaches were selected within this segment: Cornino reach, Flagogna reach, and the reach downstream of Villuzza, referred to as reaches I, II, and III, respectively (Fig. 1). Reach I was about 1 km long and was located in section C, and II and III were about 1.5 km long and were located in sections D and E, respectively. Under base-flow conditions, reach I was dominated by exposed alluvium, with multiple channels (van der Nat et al. 2002). Reach II had a predominant wandering morphology with main channels and dead sub-channels. In the main channel, there were many longitudinal and lateral bars and islands, similar to reach I (Moretto et al. 2013). In reach III, surface water infiltrates the highly permeable alluvial aquifer, and

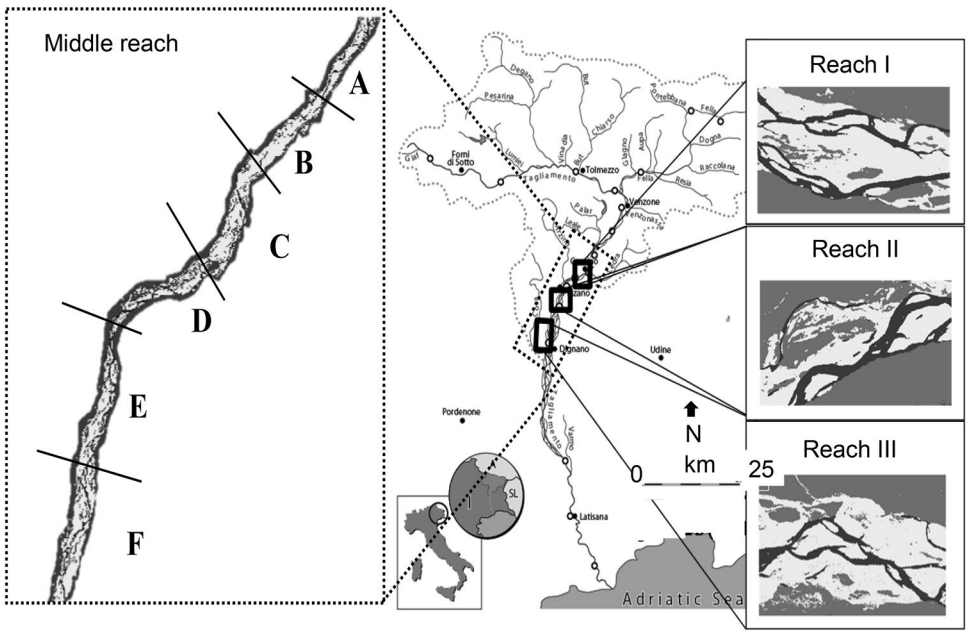

Fig. 1 The target floodplain: the middle reaches of the Tagliamento River in Northeast Italy

a portion of this segment lacks surface flow (maximum dry length: 23 km) in low-flow conditions (Doering et al. 2007; Henshaw et al. 2013).

Satellite images

Cloud cover is an important parameter when selecting satellite images for better quality data. On manual sorting of various satellite images, lower cloud cover (< 1%) was found for the September. In addition, our target was to select images of the same month for different years having at least a 10-day antecedent dry weather period to minimize the impact of precipitation on changes in habitat structure. Hence, three orthocorrected RapidEye satellite images with a 5-m spatial resolution were obtained on 12 September 2010, 30 September 2011, and 15 September 2012. All images were obtained between 10:59 and 11:03 a.m., when the cloud cover was less than 1%. A dry weather period around 10 days prior to each date was confirmed, enabling us to assume that the dynamic equilibrium of the river network was not affected by a probable flood due to precipitation. All 16-bit RapidEye satellite images consisted of four spectral bands, namely, blue, green, red, and near-infrared (NIR), with wavelengths of 440–510, 520–590, 690–730, and 760–920 nm, respectively.

Land cover classification

The maximum-likelihood classification (MLC; hereafter referred to as MLC-1), one of the most widely used methods for land cover classification, was applied to the supervised image classification (Wernick and Morris 1988); the ISODATA method (ISO) was applied to the unsupervised classification (Ball and Hall 1965; Smith et al. 2008). Several input images are required for land cover classification for both the ISO and MLC. In ISO, the pixel-value distribution of each land cover type is estimated by automatic clustering, while MLC requires training data, which are used to obtain the pixel-value distribution for each class. Generally, the accuracy is lower for ISO than for MLC using the same input images, but MLC requires reliable training data for acceptable accuracy (Smith et al. 2008).

To avoid the difficulty associated with the selection of training data in supervised classifications, in this study, a new method for quantitative image classification based on ISO was developed. In this method, when multi-spectral band images are used as input data, DN distributions for several bands can be clustered into classes because each land cover type is characterized by a different DN distribution (Bruzzone and Prieto 2001). In the conventional ISO method, hereafter referred to as ISO-1, overlapping plots and linear relationships among bands often make it difficult to accurately identify land cover classes. The proposed method for image classification, hereafter referred as ISO-2, was designed to avoid such problems in clustering by pixel-value transformation (Kojima 2011). The major improvement of this method is that the DN distribution for each class is separated owing to the increased accuracy of the ISO estimates, which minimizes overlap in the DN distribution of each class between bands in the transformed domain.

Suppose that n classes of land cover are classified based on a satellite image with M bands. The DN distribution of M bands for class i is expressed using the function f_i as follows:

$$f_i\left(\mathrm{DN}_1, \mathrm{DN}_2, \ldots \mathrm{DN}_J, \ldots, \mathrm{DN}_M\right) + \emptyset'_{i,i} = 0, \tag{1}$$

where DN_M is the DN of class i in band M and $\emptyset'_{i,i}$ is the error term equal to the deviance. According to this relation, the DN distribution of class i in band J is expressed as follows:

$$\mathrm{DN}_J(i) = g_i\left(\mathrm{DN}_1, \mathrm{DN}_2, \ldots, \mathrm{DN}_M\right) + \emptyset'_{i,i} \text{for} M \neq J, \tag{2}$$

When Eq. (2) is applied to all pixels in an image (i.e., other land cover classes), the error term differs for each class and can be expressed as a matrix as follows:

$$\emptyset'_i = \begin{bmatrix} \emptyset'_{i,1} \cdots \text{on Landcover}(1) \\ \vdots \\ \emptyset'_{i,i} \cdots \text{on Landcover}\ (i) \\ \vdots \\ \emptyset'_{i,n} \cdots \text{on Landcover}(n) \end{bmatrix}, \tag{3}$$

where $\emptyset'_i$ is the deviance distribution consisting of the errors of each class $\emptyset'_{i,n}$ obtained by applying Eq. (2) to class n.

If the image is reproduced with the deviance $\emptyset'_i$ to the pixel value, instead of DN, the deviance attributed to class i, i.e., only $\emptyset'_{i,i}$, will be closer to zero than that of other classes, since $\emptyset'_i$ is the error from the estimation equation of the DN distribution of class i. Finally, for all classes from 1 to n, the error number and DN are calculated to acquire the pixel-value distribution for each class between two images for image classification.

Application of the new classification method

To validate the DN distribution in four bands for each class, the true-color images were reproduced by combining red, green, and blue band images, and DN was selected from 30 pixels for each land cover type from this true-color image. Referring to the RapidEye sample data obtained in 2012, the DN distribution for each class was plotted and fitted to a linear spectral unmixing model for green and other bands, except the NIR band on river water (Fig. 2). Similar trends were found for each class and the other RapidEye images could be represented as follows:

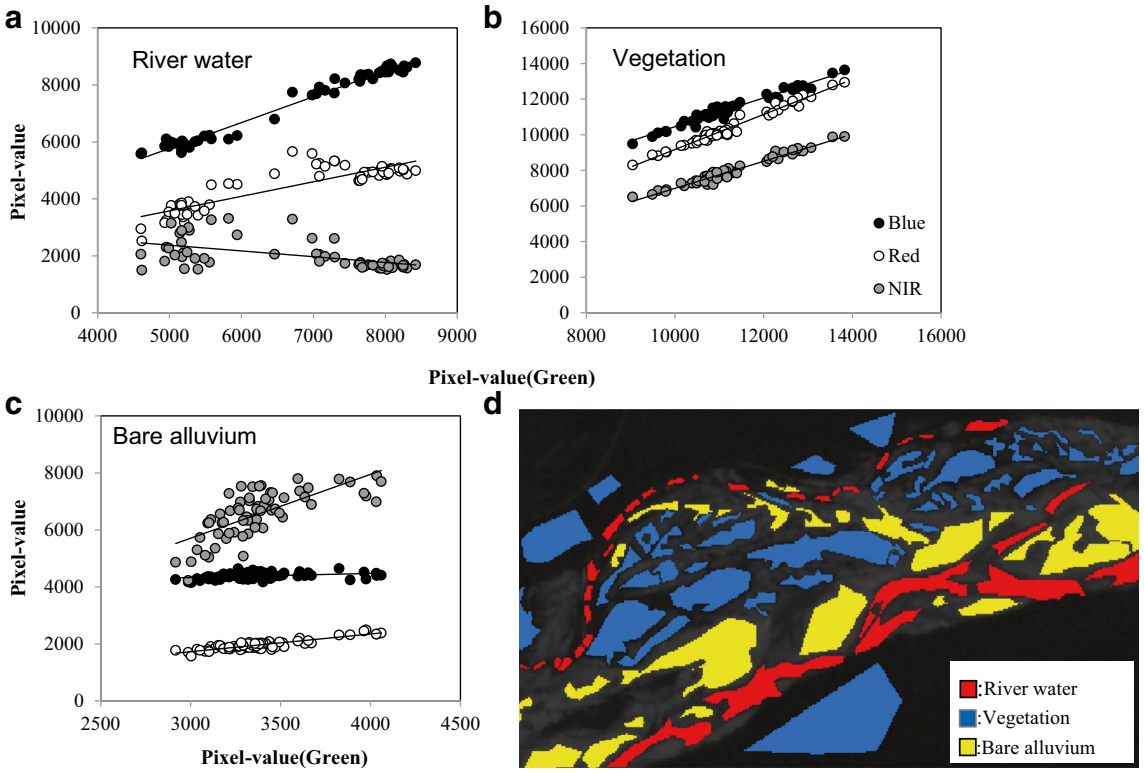

Fig. 2 The relationships of digital number distributions between green and blue, red, and near-infrared (*NIR*) for each land cover class of 2012 RapidEye satellite images: **a** river water, **b** vegetation, and **c** bare alluvium. The samples were taken from 50–100 randomly selected points of each land cover type indicated in the floodplain map (**d**). The figure parts indicate that the relationships among bands can significantly differ according to land cover type

$$\mathrm{DN}_{\mathrm{grn}}(i) = \left(a * \mathrm{DN}_{\mathrm{blue}}(i) + b * \mathrm{DN}_{\mathrm{red}}(i) + c * \mathrm{DN}_{\mathrm{NIR}}(i) + d\right) + \emptyset_i', \tag{4}$$

where $\mathrm{DN}_{\mathrm{grn}}(i)$, $\mathrm{DN}_{\mathrm{blue}}(i)$, $\mathrm{DN}_{\mathrm{red}}(i)$, and $\mathrm{DN}_{\mathrm{NIR}}(i)$ are the observed DN distributions of class i in green, blue, red, and NIR bands, respectively, and a, b, c, and d are constants. The error was estimated by applying Eq. (4) to the sample data for river water, vegetation, and bare alluvium and was used in the following ISO image classification.

In this study, image classification was conducted using GRASSGIS (version 6.4.2) for all three classification methods, namely, the conventional MLC (MLC-1), the conventional ISO (ISO-1), and the new ISO method developed in this study (ISO-2).

To check the accuracy, the omission rate, commission rate, and κ-coefficients were calculated by cross-validation using reach II. For this validation, around 50% of all pixels for each land cover were taken from true-color images. Each coefficient was estimated as follows:

$$\text{Omission rate} = \frac{1}{n_i} Q_{ij} (i \neq j), \tag{5}$$

$$\text{Commission rate} = \frac{1}{n_i} Q_{ji} (i \neq j), \tag{6}$$

$$\text{Kappa coefficient} = \frac{N \sum_{i=1}^{m} Q_{ii} - \sum_{i=1}^{m} \left(Q_{i+} \times Q_{+i}\right)}{N^2 \sum_{i=1}^{m} \left(Q_{i+} \times Q_{+i}\right)}, \tag{7}$$

where n_i is the number of pixels in class i for the validation data, Q_{ij} is the number of pixels belonging to class I but wrongly assigned to class j in the validation data, Q_{ii} is those pixels that are correctly classified, Q_{i+} is the total pixels of class i in the validation data, Q_{+i} is the total of class i in the classification result, N is the number of pixels in the whole target image, and m is the number of classes. If κ is greater than 0.80, the accuracy of the estimate is deemed sufficient (Cohen 1960; Kojima 2011).

Categorization of habitat types

The habitats in the Tagliamento River have been categorized into seven types: channel, alluvial channel, backwater, pond, bare alluvium, riparian forest, and vegetated island (van der Nat et al. 2003). As it was not possible to clearly distinguish between alluvial channels, gravel bed and bare alluvium from the RapidEye satellite images at 5-m spatial resolution, all these three habitat types were categorized as

bare alluvium. Hence, habitats in the river floodplain surrounded by riparian forest were classified into five types, namely, channels, backwaters, ponds, vegetation islands, and bare alluvium (Fig. 3).

For the fluvial habitats, ponds were defined as pools of water within the river floodplain that were not connected to any streams. Backwaters were connected to streams at only the downstream or upstream end, and the remaining river water land cover could be classified as channel. Based on the land cover estimation using satellite images, the river network was obtained; thereby, the fluvial habitat was classified morphologically into channels, backwaters, and ponds.

Estimation of the temporal shift in habitat structure

Referring to the habitat type categorization based on satellite images, the area of each habitat can be calculated as follows:

$$A_{t1}(i) = R_s^2 * N_{t1}(i), \tag{8}$$

where $A_{t1}(i)$ is the area of habitat I in period $t1$ (squared meters),R_s is the resolution of satellite images (5 m in this study), and $N_{t1}(i)$ is the number of pixels in the habitat of interest at time $t1$ on the satellite images.

To examine the temporal habitat changes after several flooding events, the conversion rate to the next time step $t2$ was represented as follows:

$$C_{t1,t2}(i,j) = A_{t2}(i,j)/A_{t1}(i), \tag{9}$$

where, $C_{t1,t2}(i,j)$ is the conversion rate of habitat type i to j between the period from $t1$ to $t2$, $A_{t2}(i,j)$ is the area of habitat type j converted from type i, and $A_{t1}(i)$ is the area of habitat type i at time $t1$. In this study, the conversion rate was calculated for each habitat change from 2010 to 2011 and from 2011 to 2012 in three reaches.

To understand the habitat changes (or lack thereof) over several years, the rate of unchanged habitat for each type was also calculated by overlaying the habitat type classification images for each year using the following function:

$$U_{\mathrm{tn}}(i) = A_{t1}(i) \cap A_{t2}(i) \cap \cdots \cap A_{tn}(i)/A_{t1}(i), \tag{10}$$

where $U_{tn}(i)$ represents unchanged habitat type i over the period from $t1$ to tn.

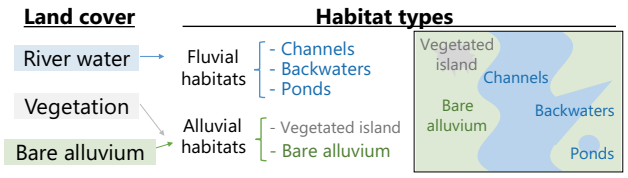

Fig. 3 Categorization of land cover and habitat types of the Tagliamento River

Results and discussion

Land cover classification

All parameters of Eq. (4) were obtained from the DN distribution estimates for four bands as shown in Table 1 and Fig. 2. The correlations between each estimate and observation exceeded 0.90. High-resolution satellite images showed higher correlation coefficients and the highest value was obtained for bare alluvium, with a maximum of 0.99 (Fig. 2). The DN distribution of 50–100 randomly selected pixels of Fig. 2d is reflected in Fig. 2a–c, which was obtained after merging the frequency distribution of river water, vegetation and bare alluvium in the blue, red, green and NIR bands (Supplementary Fig. S1), and the frequency distribution of the blue, red, green and NIR bands for river water, vegetation and bare alluvium for the 2012 image (Supplementary Fig. S2).

According to the pixel-value distributions for the RapidEye satellite image obtained in 2012, the distributions of each class partially overlapped using both ISO-1 and ISO-2 (Fig. 4). However, for ISO-1, the DN distributions of river water, vegetation, and bare alluvium totally overlapped, as DNs were plotted on the same line for the blue, green, and red bands, whereas ISO-2 did not show such an overlap. In addition, the pixel-value distributions for ISO-2 were closer to zero than those of ISO-1 when the estimation class was objective and the distributions were the same (Fig. 4). The plots of each land cover type for ISO-1 were similar, especially among neighboring bands, except for red and NIR.

Table 1 Parameter estimates for the digital number correlation equation

	2010				2011				2012			
	a	b	c	d	a	b	c	d	a	b	c	d
River water	0.71	0.36	− 0.20	− 0.19	0.38	0.68	0.08	0.00	0.94	0.20	− 0.09	− 933
Vegetation	0.12	0.93	0.08	− 566	0.19	0.64	0.08	784	− 0.06	1.07	0.08	1009
Bare alluvium	0.34	0.43	0.35	0.00	0.38	0.53	0.18	0.00	0.46	0.28	0.43	− 455

Please refer to Eq. 4. The values of a, b, c and d correspond with those of the test sites as shown in the figure parts of Fig. 2

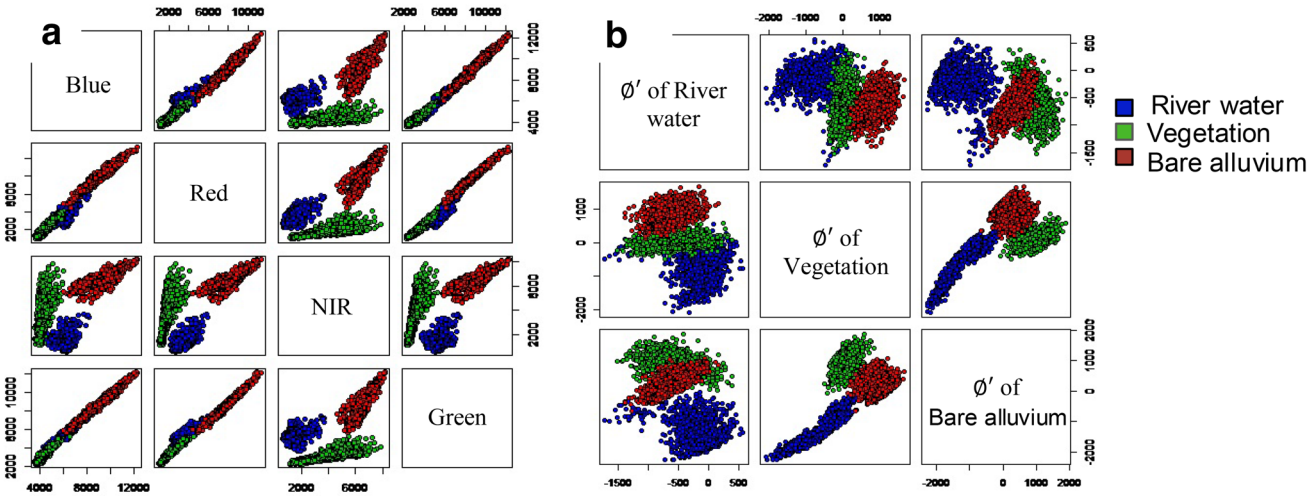

Fig. 4 Pixel-value distribution in input images for 2012 using **a** the conventional ISODATA (ISO-1) and **b** the proposed ISODATA method (ISO-2) (the same numbers of pixel values were selected for comparison between **a** and **b**)

This means that the classes cannot be effectively separated and thus linear plots make clustering difficult.

The differences in image classification based on the pixel-value distribution among input images, overlapping for ISO-1 and less overlapping (or no overlapping) for ISO-2, were also supported by the higher κ-coefficient for ISO-2 (Table 2). The κ-coefficient was greater than 0.89, exceeding a reference threshold of 0.80, indicating better efficiency for ISO-2 for all images obtained in 2010, 2011, and 2012. Hence, in this study, the distribution of pixels based on the newly developed method showed a better ability to isolate river water, vegetation, and bare alluvium land covers.

In the land cover classification results, the κ-coefficient exceeded 0.83, a sufficient threshold value, for ISO-1, ISO-2,

Table 2 Commission rate, omission rate, and κ-coefficient of land cover classification for each year

2010	MLC-1		ISO-1		ISO-2	
κ	87.6		83.1		89.9	
	Commission	Omission	Commission	Omission	Commission	Omission
River water	0.6	4.5	33.7	6.1	1.4	3.0
Vegetation	2.0	14.4	2.9	19.9	1.2	11.9
Bare alluvium	17.9	0.0	1.5	0.1	15.0	0.0
2011	MLC-1		ISO-1		ISO-2	
κ	97.0		95.6		98.7	
	Commission	Omission	Commission	Omission	Commission	Omission
River water	0.0	2.0	11.1	1.7	0.2	2.3
Vegetation	0.3	3.1	0.7	5.0	0.6	0.7
Bare alluvium	4.5	0.0	0.1	0.2	1.4	0.0
2012	MLC-1		ISO-1		ISO-2	
κ	95.1		93.1		95.6	
	Commission	Omission	Commission	Omission	Commission	Omission
River water	0.1	3.2	16.0	2.5	0.1	4.2
Vegetation	1.3	5.0	1.1	7.4	0.9	4.0
Bare alluvium	7.4	0.1	0.0	0.8	7.0	0.0

MLC-1 Conventional maximum-likelihood classification, *ISO-1* conventional ISODATA method, *ISO-2* proposed ISODATA method

and MLC-1 (Table 2). The κ-values for ISO-2 were 0.89, 0.98, and 0.95 for 2010, 2011, and 2012, respectively. Similarly, the κ-values for MLC-1 were 0.87, 0.97, and 0.95 for 2010, 2011, and 2012, respectively. The values of κ from the ISO-1 classification were 0.83, 0.95, and 0.93 for the same years, respectively.

The outputs obtained by image classification for ISO-1 indicated that the river water data were overestimated and the boundaries between each land cover type were ambiguous (Fig. 4). The boundaries among each land cover were clear in ISO-2 and MLC-1 (Fig. 4). The results for vegetation differed between ISO-2 and MLC-1. ISO-2 was apparently able to estimate vegetation at a finer scale than MLC-1, especially in 2010 and 2011 (Fig. 4). Similar trends to those in reach II were found in reach I and III.

Therefore, the developed method (ISO-2) enables more accurate estimates of the land cover class without a repetitive data-selection training process than the conventional unsupervised method (ISO-1), as the pixel values were clearly differentiable among river water, vegetation, and bare alluvium in the Tagliamento River. In addition, the accuracy of the newly developed method was high, i.e., greater than 89%. However, it is necessary to validate the efficiency of this new method for other land cover classes (e.g., urban areas), and the efficiency for the classification of types of soil, vegetation, and plants should be evaluated in further studies.

Spatiotemporal land cover changes

Referring to the land cover classification results, the land cover ratio and the unchanged area in the floodplain surrounded by riparian forests were obtained from 2010 to 2012 in the middle reaches of the Tagliamento River (Fig. 5). The presence of vegetation was relatively low in areas A and B in the upper part of the Tagliamento River and higher in area D, the middle part, which includes reach II. The presence of river water was higher in the middle region (namely, areas C, D, and E, which include reach I and II) than in other regions (Fig. 5a). The rate of unchanged river water in each area was also calculated (Fig. 5b) and was higher in area D for all periods from 2010 to 2011, 2011 to 2012, and 2010 to 2012, probably due to the presence of dead subchannels in reach II

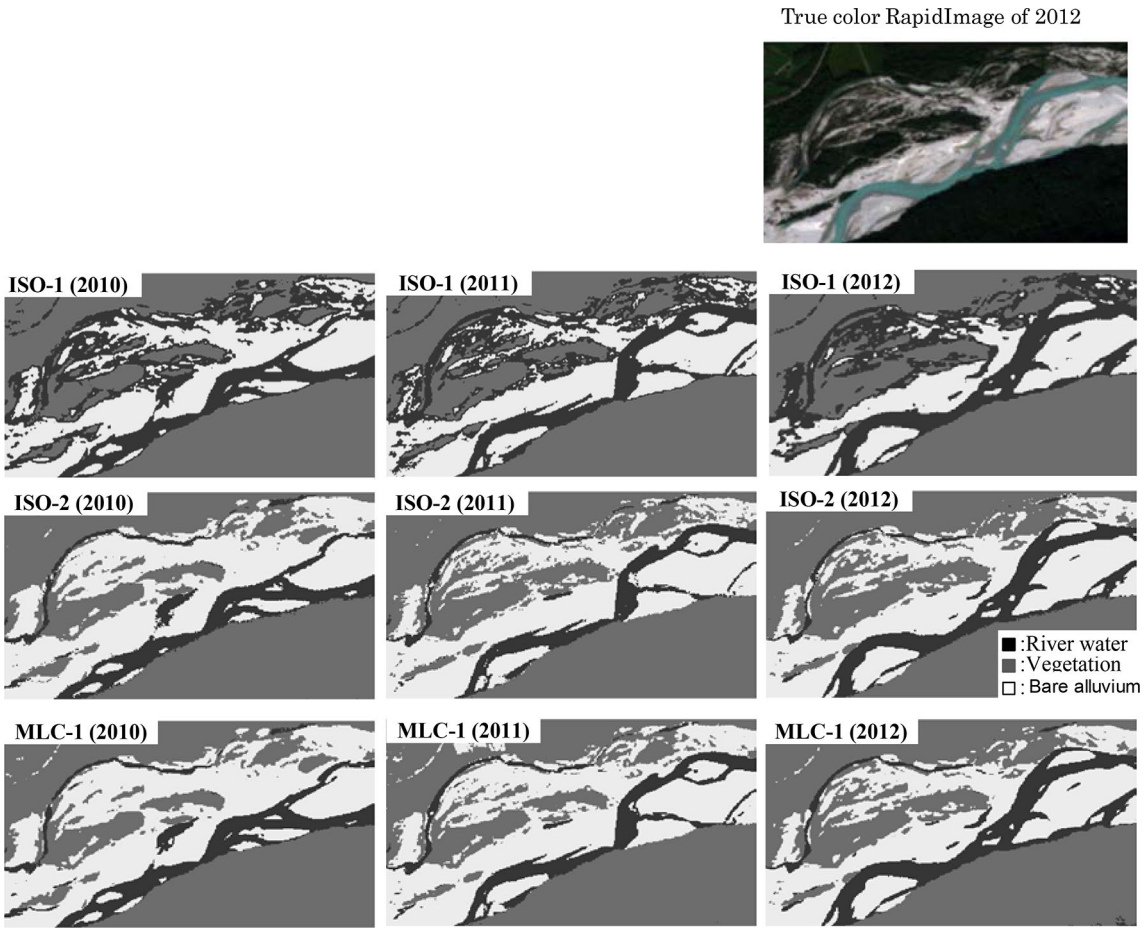

Fig. 5 Outputs obtained by the image classification of ISO-1, ISO-2, and conventional maximum-likelihood classification (*MLC-1*) from 2010 to 2012 in reach II, and true-color RapidImage in 2012 (*top right*)

(Moretto et al. 2013). In all areas, the unchanged area was greater for 2011 to 2012 than 2010 to 2011, and in the lower part (areas D, E, and F), the unchanged area decreased in the downstream direction for all periods.

Based on the composition of habitat types obtained from the land cover classification, the dominant habitat type was bare alluvium, covering 55–75% of each reach (Fig. 6). The unchanged area was highest for vegetated

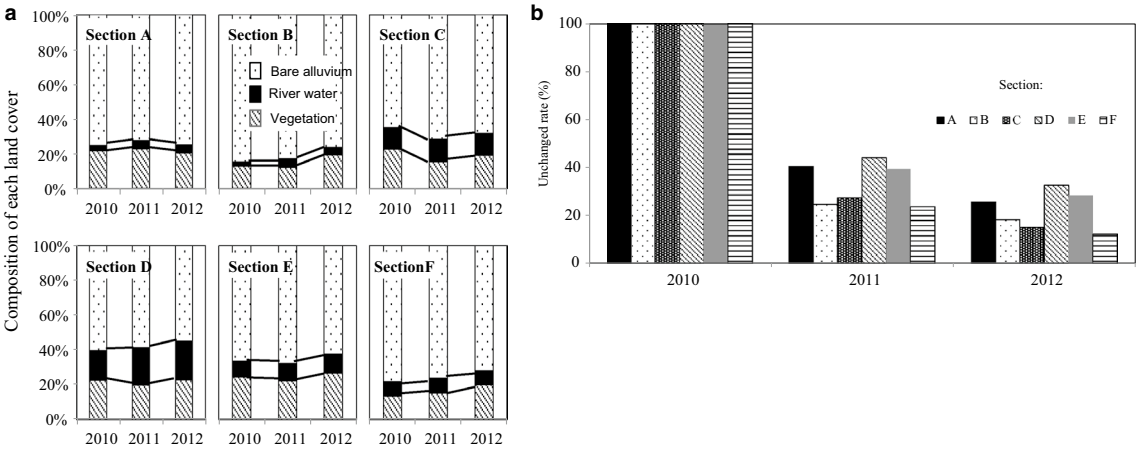

Fig. 6a, b Temporal shift of each habitat. **a** Composition of each land cover type in the middle of the Tagliamento River, and **b** unchanged river water in the middle of the Tagliamento River

Table 3 Annual habitat turnover from 2010 to 2011 and from 2011 to 2012

Reach I	September 2010						September 2011				
September 2011	CH	BW	PD	VI	BA	September 2012	CH	BW	PD	VI	BA
CH	31.7	11.8	0.0	4.6	9.7	CH	55.7	38.9	31.6	3.2	14.1
BW	2.2	1.1	23.5	0.5	1.1	BW	4.2	12.8	21.1	0.2	1.2
PD	0.1	0.2	0.0	0.0	0.1	PD	0.0	0.0	0.0	0.1	0.1
VI	0.6	0.0	0.2	71.1	3.2	VI	0.2	0.4	0.0	90.3	3.1
BA	65.3	86.9	76.3	23.8	85.8	BA	39.9	47.9	47.4	6.2	81.6
Reach II	September 2010						September 2011				
September 2011	CH	BW	PD	VI	BA	September 2012	CH	BW	PD	VI	BA
CH	44.6	18.1	0.0	5.7	10.5	CH	64.5	48.5	0.0	2.5	12.6
BW	0.0	3.6	0.0	0.1	0.9	BW	1.3	0.0	0.0	0.0	0.1
PD	0.0	5.7	9.9	0.2	0.3	PD	0.1	0.0	17.8	0.1	0.8
VI	1.0	0.4	2.9	87.5	13.2	VI	1.5	0.0	7.9	91.4	5.3
BA	54.4	72.2	87.2	6.5	75.1	BA	32.7	51.5	74.3	6.0	81.2
Reach III	September 2010						September 2011				
September 2011	CH	BW	PD	VI	BA	September 2012	CH	BW	PD	VI	BA
CH	27.1	64	0.0	4.2	12.4	CH	56.8	39.6	0.0	3.9	16.9
BW	0.8	0.0	0.0	0.2	1.2	BW	1.5	14.1	0.0	0.0	0.8
PD	2.2	0.0	0.0	0.0	0.1	PD	0.0	0.0	20.3	0.0	0.3
VI	0.5	0.0	1.3	69.9	3.7	VI	0.2	0.0	0.0	78.5	0.7
BA	69.4	36	98.7	25.7	82.6	BA	41.5	46.2	46.2	17.6	81.3

CH Channels, *BW* backwaters, *PD* ponds, *VI* vegetative islands, *BA* bare alluvium

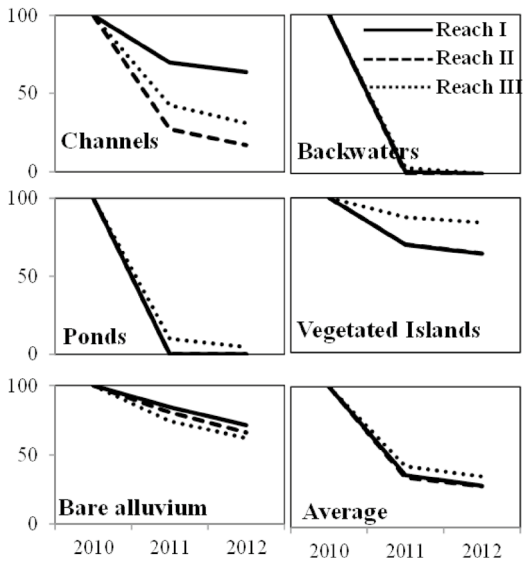

Fig. 7 Unchanged rate (%) of each habitat type from 2010 to 2012

Unchanged rate (%)

$$= \frac{A_{t1}(i) \cap A_{t2}(i) \cap \cdots \cap A_{tn}(i)}{A_{t1}(i)} * 100$$

where $A_{t1}(i)$ is the total area of habitat type(i) on t1 (=2010).

Habitat at 2010 is considered as unchanged and is set as 100%.

Please refer to equation 10 for details

islands (19.4–26.5%) in reach II, and lowest (7.5–8.7%) in reach III. Table 3 shows the annual habitat turnover from 2010 to 2011 and 2011 to 2012 in reaches I, II, and III, respectively. The unchanged area of fluvial habitats, such as channels, backwaters, and ponds, exhibited random patterns in the three reaches. For instance, the unchanged area of channels was highest in reach I (31.7 and 55.7%), II (44.6 and 64.5%), and III (64 and 56.8%) for 2010 to 2011 and 2011 to 2012 (Table 3).

The observed turnover was explained by two main factors, i.e., flooding, which usually occurs around ten times per year in the Tagliamento River, and gradual changes associated with the seasonal changes in discharge. These are both important processes determining habitat properties and faunal species richness (Benke et al. 2000; Tockner et al. 2000). Since the RapidEye images used in this study were obtained within a half-month period each year, the extrapolation of the present results to other seasons should be done with care, as seasonal variation in vegetation has been reported in an earlier study in the Tagliamento River (Doering et al. 2007).

The unchanged area was highest for bare alluvium in reaches I and III and for vegetated islands in reach II (Fig. 6). For fluvial habitats, especially in channels, the unchanged area was highest in reach II. This is explained by the high proportion of unchanged area in the subchannel in reach II, i.e., 75% from 2010 to 2011 and 66% over 2 years, compared with the averages of 33 and 20% for all reaches, respectively. These surviving patches may serve as refuges for benthic macroinvertebrates during floods or increasing discharge. Such refuges play important roles in the recolonization of newly formed habitats after a flood (Sedell et al. 1990; Robertson et al. 1995; Winterbottom et al. 1997; Rempel et al. 1999).

Variability in habitat abundance and channel complexity is associated with changes in water and sediment supply, flooding, and vegetation-driven stabilization processes (Kiss et al. 2008). According to the results of this study, the habitat distribution exhibits spatial and temporal changes, especially for fluvial habitats, while the composition of habitat types is roughly constant in the middle reaches of the Tagliamento. These findings are consistent with those of previous studies (Arscott et al. 2002; van der Nat et al. 2003). The high-resolution satellite image classification system developed in this study enables the continuous monitoring of the spatiotemporal dynamics of habitat structures at a larger spatial scale and a higher accuracy (> 89%) than those of field observations (Fig. 7).

Conclusion

The dynamics of habitat structures in floodplains located in the middle reaches of the Tagliamento River were estimated using high-resolution satellite images, i.e., multi-spectral images of RapidEye at a spatial resolution of 5 m. This estimation facilitates discussion of the annual turnover of floodplain habitat structure from 2010 to 2012. A major advantage of the image classification method developed in this study is that it does not require empirical training with data and additional observations while covering the changes in habitat structure at such a large spatiotemporal scale with high resolution; hence, it is relatively simple, easy to implement, and accurate (> 89%) compared to the conventional method. The specific conclusions of this study are as follows.

- Three classes of land cover in the Tagliamento River floodplain were identified: river water, vegetation, and bare alluvium.
- The unchanged area of vegetation was relatively small in the lower part and bigger in the middle part of the river, and unchanged river water was higher in the middle part of the Tagliamento River. In all areas, the rate of unchanged habitat was greater for 2011–2012 than for 2010–2011.
- The dominant habitat type was bare alluvium, covering 55–75% of each reach. The rate of unchanged vegetated islands was highest (19.4–26.5%) in reach II and lowest (7.5–8.7%) in reach III. Unchanged habitat was highest for bare alluvium and vegetated islands.
- The habitat distribution exhibited spatial and temporal changes, especially for fluvial habitats. The composition of habitat type was preserved in the middle reaches of the Tagliamento River.
- For future research, since the resolution and observation frequency of satellite images are constantly improving, the detailed and comprehensive monitoring of habitat structures, especially in urban areas, and the classification of soil, vegetation, and plant types are recommended. More effective river-floodplain monitoring could be developed by integrating the accurate method developed in this study, images with a higher resolution, and field observations.

Acknowledgments The authors would like to thank Drs Yasuhiro Takemon, Kozo Watanabe, Takeo Tadono and Sayaka Yoshikawa for their constructive comments, which helped us polish this manuscript. This research was supported by Japan Society for the Promotion of Science Kakenhi grants (numbers JP25241024, JP15K00592) and partly by JST/JICA, SATREPS.

References

Arscott DB, Tockner K, van der Nat D, Ward JV (2002) Aquatic habitat dynamics along a braided alpine river ecosystem (Tagliamento River, Northeast Italy). Ecosystems 5:802–0814

Arscott DB, Tockner K, Ward JV (2005) Lateral organization of aquatic invertebrates along the corridor of a braided floodplain river. J N Am Benthol Soc 24:934–954

Ball GH, and Hall DJ (1965) ISODATA, a novel method of data analysis and pattern classification. Technical report NTIS AD 699616. Stanford Research Institute, CA

Belmar O, Bruno D, Martínez-Capel F, Barquín J, Velasco J (2013) Effects of flow regime alteration on fluvial habitats and riparian quality in a semiarid Mediterranean basin. Ecol Indic 30:52–64

Benke AC, Chaubey I, Ward GM, Dunn EL (2000) Flood pulse dynamics of an unregulated river floodplain in the southeastern U.S. coastal plain. Ecology 81:2730–2741

Bertoldi W, Gurnell A, Surian N, Tockner K, Zanoni L, Ziliani L, Zolezzi G (2009) Understanding reference processes: linkages between river flows, sediment dynamics and vegetated landforms along the Tagliamento River, Italy. River Res Appl 25:501–516

Bertoldi W, Zanoni L, Tubino M (2010) Assessment of morphological changes induced by flow and flood pulses in a gravel bed braided river: the Tagliamento River (Italy). Geomorphol 114:348–360

Bruzzone L, Prieto DF (2001) Unsupervised retraining of a maximum likelihood classifier for the analysis of multitemporal remote sensing images. IEEE J Geosci Remote Sens 39:456–460

Bryant RG, Gilvear DJ (1999) Quantifying geomorphic and riparian land cover changes either side of a large flood event using airborne remote sensing: River Tay, Scotland. Geomorphol 29:307–321

Cohen J (1960) A coefficient of agreement for nominal scales. Educ Psychol Meas 20:37–46

Cornell HV, Lawton JH (1992) Species interactions, local and regional processes, and limits to the richness of ecological communities—a theoretical perspective. J Anim Ecol 61:1–12

Doering M, Uehlinger U, Rotach A, Schlaepfer DR, Tockner K (2007) Ecosystem expansion and contraction dynamics along a large Alpine alluvial corridor (Tagliamento River, Northeast Italy). Earth Surf Process Landf 32:1693–1704

Dufour S, Bernez I, Betbeder J, Corgne S, Hubert-Moy L, Nabucet J, Rapinel S, Sawtschuk J, Trollé C (2013) Monitoring restored riparian vegetation: how can recent developments in remote sensing sciences help? Knowl Manag Aquat Ecosyst 410:10

Edwards PJ, Kollmann J, Gurnell AM, Petts GE, Tockner K, Ward JV (1999) A conceptual model of vegetation dynamics on gravel bars of a large Alpine river. Wetl Ecol Manage 7:141–153

García A, Jorde K, Habit E, Caamaño D, Parra O (2011) Downstream environmental effects of dam operations: changes in habitat quality for native fish species. River Res Appl 27:312–327

Gunawardhana LN, Kazama S (2012) A water availability and low-flow analysis of the Tagliamento River discharge in Italy under changing climate conditions. Hydrol Earth Syst Sci 16:1033–1045

Gurnell AM, Petts GE, Hannah DM, Smith BP, Edwards PJ, Kollmann J, Ward JV, Tockner K (2001) Riparian vegetation and island formation along the gravel-bed Fiume Tagliamento, Italy. Earth Surf Process Landf: J Br Geomorphol Res Group 26:31–62

Henshaw AJ, Gurnell AM, Bertoldi W, Drake NA (2013) An assessment of the degree to which Landsat TM data can support the assessment of fluvial dynamics, as revealed by changes in vegetation extent and channel position, along a large river. Geomorphol 202:74–85

Hinojosa-Huerta O, Nagler PL, Carrillo-Guererro YK, Glenn EP (2013) Effects of drought on birds and riparian vegetation in the Colorado River Delta, Mexico. Ecol Eng 51:275–281

Huber E, Huggenberger P (2015) Morphological perspective on the sedimentary characteristics of a coarse, braided reach: Tagliamento River (NE Italy). Geomorphol 248:111–124

Itakura H, Kitagawa T, Miller MJ, Kimura S (2015) Declines in catches of Japanese eels in rivers and lakes across Japan: have river and lake modifications reduced fishery catches? Landsc Ecol Eng 11:147–160

Jensen JR (1996) Introductory digital image processing. A remote sensing perspective. Prentice Hall, Upper Saddle River

Kanno A, Koibuchi Y, Isobe M (2011) Statistical combination of spatial interpolation and multispectral remote sensing for shallow water bathymetry. IEEE Geosci Remote Sens Lett 8:64–67

Kiss T, Fiala K, Sipos G (2008) Alterations of channel parameters in response to river regulation works since 1840 on the Lower Tisza River (Hungary). Geomorphol 98:96–110

Kojima N (2011) Evaluation method of image classification accuracy. In: Tateishi R (ed) The understanding of basic remote sensing techniques. Rikotosho, Tokyo, pp 247–252 **(in Japanese)**

Legleiter CJ, Roberts DA, Marcus WA, Fonstad MA (2004) Passive optical remote sensing of river channel morphology and in-stream habitat: physical basis and feasibility. Remote Sens Environ 93:493–510

Marcus WA, Fonstad MA (2008) Optical remote mapping of rivers at sub-meter resolutions and watershed extents. Earth Surf Process Landf 33:4–24

Marcus WA, Fonstad MA (2010) Remote sensing of rivers: the emergence of a subdiscipline in the river sciences. Earth Surf Process Landf 35:1867–1872

Melack JM, Hess LL (2010) Remote sensing of the distribution and extent of wetlands in the Amazon basin. In: Junk W, Piedade M, Wittmann F, Schöngart J, Parolin P (eds) Amazonian floodplain forests. Springer, Dordrecht, pp 43–59

Mertes LA (2002) Remote sensing of riverine landscapes. Freshwater Biol 47(4):799–816

Moretto J, Delai F, Picco L, Lenzi MA (2013) Integration of colour bathymetry, LiDAR and dGPS surveys for assessing fluvial changes after flood events in the Tagliamento River (Italy). Agric Sci 4(8A):21–29

Müller N (1996) River dynamics and floodplain vegetation and their alterations due to human impact. Large Rivers 9:477–512

Nessimian JL, Venticinque EM, Zuanon J, De Marco P, Gordo M, Fidelis L, Batista JDA, Juen L (2008) Land use, habitat integrity, and aquatic insect assemblages in Central Amazonian streams. Hydrobiologia 614:117–131

Osugi T, Tate SI, Takemura K, Watanabe W, Ogura N, Kikkawa J (2007) Ecological research for the restoration and management of rivers and reservoirs in Japan. Landsc Ecol Eng 3:159–170

Rempel LL, Richardson JS, Healey MC (1999) Flow refugia for benthic macroinvertebrates during flooding of a large river. J N Am Benthol Soc 18:34–48

Robertson AL, Lancaster J, Hildrew AG (1995) Stream hydraulics and the distribution of microcrustacea: a role for refugia? Freshwater Biol 33:469–484

Romero A, Gatta C, Camps-Valls G (2016) Unsupervised deep feature extraction for remote sensing image classification. IEEE Trans Geosci Remote Sens 54:1349–1362

Rosgen DL (1994) A classification of natural rivers. CATENA 22:169–199

Schneider J, Grosse G, Wagner D (2009) Land cover classification of tundra environments in the Arctic Lena Delta based on Landsat 7 ETM + data and its application for upscaling of methane emissions. Remote Sens Environ 113:380–391

Sedell JR, Reeves GH, Hauer FR, Stanford JA, Hawkins CP (1990) Role of refugia in recovery from disturbances: modern fragmented and disconnected river systems. Environ Manage 14:711–724

Smith TM, Reynolds RW, Peterson TC, Lawrimore J (2008) Improvements to NOAA's historical merged land–ocean surface temperature analysis (1880–2006). J Clim 21:2283–2296

Spaliviero M (2003) Historic fluvial development of the Alpine-foreland Tagliamento River, Italy, and consequences for floodplain management. Geomorphol 52:317–333

Thomaz SM, Bini LM, Bozelli RL (2007) Floods increase similarity among aquatic habitats in river-floodplain systems. Hydrobiologia 579:1–13

Tilman D (1999) The ecological consequences of changes in biodiversity: a search for general principles. Ecology 80:1455–1474

Tockner K, Schiemer F, Baumgartner C, Kum G, Weigand E, Zweimüller I, Ward JV (1999) The Danube restoration project: species diversity patterns across connectivity gradients in the floodplain system. Regul Rivers: Res Manage 15:245–258

Tockner K, Malard F, Ward JV (2000) An extension of the flood pulse concept. Hydrol Process 14:2861–2883

Tockner K, Ward JV, Arscott DB, Edwards PJ, Kollmann J, Gurnell AM, Petts GE, Maiolini B (2003) The Tagliamento River: a model ecosystem of European importance. Aquat Sci 65:239–253

Tockner K, Bunn S, Gordon C, Naiman RJ, Quinn GP, Stanford JA (2008) Flood plains: critically threatened ecosystems. In: Polunin NVC (ed) Aquatic ecosystems. Cambridge University Press, Cambridge, pp 45–61

Tockner K, Lorang MS, Stanford JA (2010) River flood plains are model ecosystems to test general hydrogeomorphic and ecological concepts. River Res Appl 26:76–86

van der Nat D, Schmidt AP, Tockner K, Edwards PJ, Ward JV (2002) Inundation dynamics in braided floodplains: Tagliamento River, northeast Italy. Ecosystems 5:636–647

van der Nat D, Tockner K, Edwards PJ, Ward JV, Gurnell AM (2003) Habitat change in braided flood plains (Tagliamento NEiamento). Freshwater Biol 48:1799–1812

Ward JV, Tockner K, Schiemer F (1999) Biodiversity of floodplain river ecosystems: ecotones and connectivity. Regul Rivers: Res Manage 15:125–139

Wernick MN, Morris GM (1988) Maximum-likelihood image classification. Proc. SPIE Digital Optical Shape Represent Pattern Recognit 938:317–321

Whited DC, Kimball JS, Lorang MS, Stanford JA (2013) Estimation of juvenile salmon habitat in Pacific Rim rivers using multiscalar remote sensing and geospatial analysis. River Res Appl 29:135–148

Winterbottom JH, Orton SE, Hildrew AG, Lancaster J (1997) Field experiments on flow refugia in streams. Freshwater Biol 37:569–580

Xue Z, Liu JP, Ge Q (2011) Changes in hydrology and sediment delivery of the Mekong River in the last 50 years: connection to damming, monsoon, and ENSO. Earth Surf Process Landf 36:296–308